JNeurosci
THE JOURNAL OF NEUROSCIENCE

Research Articles: Cellular/Molecular

Biphasic modulation of NMDA receptor function by metabotropic glutamate receptors

Nathanael O'Neill[1], Catherine McLaughlin[1], Noboru Komiyama[1,2] and Sergiy Sylantyev[1,3]

[1]*Centre for Clinical Brain Sciences, University of Edinburgh, 49 Little France Crescent, EH16 4SB, Edinburgh, UK.*

[2]*Centre for Neuroregeneration, University of Edinburgh, 49 Little France Crescent, EH16 4SB, Edinburgh, UK.*

[3]*Department for Clinical & Experimental Epilepsy, Institute of Neurology, UCL, Queen Square, London WC1N 3BG, UK.*

DOI: 10.1523/JNEUROSCI.1000-18.2018

Received: 18 April 2018

Revised: 2 September 2018

Accepted: 9 September 2018

Published: 3 October 2018

Author contributions: N.O., C.M., and S.S. performed research; N.O., N.K., and S.S. analyzed data; N.O. edited the paper; N.K. contributed unpublished reagents/analytic tools; S.S. designed research; S.S. wrote the paper.

Conflict of Interest: The authors declare no competing financial interests.

This work was supported by the RS MacDonald Seedcorn Grant 2017 and Wellcome Trust - UoE ISSF Award to S.S. Authors thank Prof. Dmitri Rusakov (UCL) for valuable suggestions on paper preparation.

Corresponding author: s.sylantyev@ed.ac.uk

Cite as: J. Neurosci ; 10.1523/JNEUROSCI.1000-18.2018

Biphasic modulation of NMDA receptor function by metabotropic glutamate receptors

Running title: Biphasic mGluRI-NMDAR crosstalk

Nathanael O'Neill[1], Catherine McLaughlin[1], Noboru Komiyama[1,2], Sergiy Sylantyev[1,3,*]

[1] – Centre for Clinical Brain Sciences, University of Edinburgh, 49 Little France Crescent, EH16 4SB, Edinburgh, UK.

[2] – Centre for Neuroregeneration, University of Edinburgh, 49 Little France Crescent, EH16 4SB, Edinburgh, UK.

[3] – Department for Clinical & Experimental Epilepsy, Institute of Neurology, UCL, Queen Square, London WC1N 3BG, UK.

* – Corresponding author: s.sylantyev@ed.ac.uk

Abstract

A recently reported rapid potentiation of NMDA receptors by group I metabotropic glutamate receptors (mGluRIs) via a Homer protein link is distinct from the classical, relatively slow inhibitory G-protein-associated signalling triggered by mGluRIs activation. The relationship between these two mechanisms remains unknown.

Here, we focused on the mGluRI-dependent modulation of NMDAR response in hippocampal dentate gyrus granule cells (DGCs) and cerebellar granule cells (CGCs) of C57BL6-J mice and found that these two contrasting mechanisms overlap competitively on the time scale from hundreds of milliseconds to seconds, with the net effect depending on the cell type. At a shorter time interval (units of millisecond) the Homer-mediated signal from mGluRIs prevails, causing upregulation of NMDAR function, in both DGCs and CGCs. Our results shed light on the possible mechanisms of anti-schizophrenia drugs that disrupt Homer-containing protein link.

Key words: metabotropic glutamate receptors, NMDA receptors, dentate gyrus granule cells, cerebellar granule cells, inter-receptor crosstalk, Homer protein.

Significance statement

Here we study modulation of N-methyl-D-aspartate receptors (NMDARs) triggered by activation of metabotropic glutamate receptors group I (mGluRIs) via two distinct pathways: classical G-protein signalling system and newly discovered high-speed modulatory mechanism associated with Homer-protein-containing direct molecular link. We found that these two contrasting mechanisms overlap competitively on the time scale from hundreds of milliseconds to seconds, with the net effect depending on the cell type. We have also found that both crosstalk mechanisms cause significant changes in synaptic strength and plasticity.

Our results resolve an apparent discrepancy between earlier studies that demonstrated contradictive effects of Homer-containing protein link disruption on NMDAR signalling. On top of that, our data provide a plausible explanation for unclear action mechanisms of anti-schizophrenia drugs.

Introduction

Neuronal metabotropic glutamate receptors group I (mGluRIs) are classically viewed as the modulators (predominantly augmentative) of N-methyl-D-aspartate receptors (NMDARs); G-protein signalling cascades are the transfer mechanism of this modulation (Rossi et al., 1996; Kunishima et al., 2000; Pin and Acher, 2002). This signalling mechanism can be interrupted by blocking various stages of the G-protein cascade. Pertussis toxin (PeTX) acts as a blocker of G_i, G_o, and G_t proteins (Kost et al., 1999), enabling research of the mGluRI-NMDAR interaction cleared from G-protein signalling effects.

The second, more recently discovered, mechanism of mGluRI-NMDAR crosstalk is signal transfer via the Homer proteins. Homer protein family contains a C-terminal coiled-coil dimerization domain ('long' Homers), except for Homer1a and Ania-3 ('short' Homers), which lack this domain and, as a result, are unable to perform a scaffolding role linking other proteins. Homer proteins bind to the mGluRIs (Brakeman et al., 1997), and to the proteins of the Shank family (Tu et al., 1999). The Shank proteins, in turn, connect to NMDARs via the protein PSD-95, establishing a direct molecular link between mGluRIs and NMDARs (Bertaso et al., 2010). Overexpressed Homer1a disrupts mGluRI-NMDAR protein connection by outcompeting "long" Homers on the binding site of mGluRIs, thus providing an experimental approach where the mGluRI-NMDAR modulation signal can pass through cytoplasmic biochemical cascades only.

We have previously shown that at a short time scale (low milliseconds) mGluRIs activation in cerebellar granule cells (CGCs) potentiates NMDARs in intact cells, but has no effect when the Homer molecular interlink has been disrupted by Homer1a overexpression (Sylantyev et al., 2013). An earlier study, however, showed that at longer intervals (hundreds of milliseconds to seconds), the activation of mGluRIs in CGCs does not affect NMDARs when the Homer scaffold is intact, but depresses NMDAR responses when the Homer-containing interlink is abolished, i.e. mGluRI-NMDAR modulatory signal is delivered exclusively through G-protein cascades (Bertaso et al., 2010). In contrast, long-term NMDAR effects were repeatedly shown to be potentiated by mGluRIs in experimental cell systems (Xenopus oocytes) (Skeberdis et al., 2001) and in brain areas other than the cerebellum, such as the subthalamic nucleus (Awad et al., 2000) and hippocampus (Harvey and Collingridge, 1993; Fitzjohn et al., 1996; Naie and Manahan-Vaughan, 2004).

It has been widely accepted that NMDAR hypofunction is one of the key factors provoking schizophrenia development (Steullet et al., 2016; Nakazawa et al., 2017). Another important element, in which dysfunction is tightly associated with the propagation of schizophrenia, are mGluRIs (Cleva and Olive, 2011). In particular, the inhibition of metabolic signalling delivered by G-proteins has been implicated in propagating schizophrenia symptoms (Chowdari et al., 2002; Williams et al., 2004). In turn, Homer1-knockout animals, in which a direct mGluRI-NMDAR link is

absent, exhibit a wide spectrum of abnormalities that are consistent with schizophrenia symptoms (Szumlinski et al., 2005), thus suggesting Homer as an actor preventing schizophrenia development. However, anti-schizophrenia drugs such as haloperidol and clozapine upregulate the synthesis of Homer1a protein, which destroys the Homer-containing mGluRI-NMDAR link (Polese et al., 2002).

Here, we aimed to resolve these apparent functional discrepancies, and to clarify the interaction of overlapping signals delivered through (a) rapid Homer-mediated and (b) slower G-protein-mediated pathways of mGluRI-NMDAR crosstalk. We hypothesised that mGluRIs, when activated, could modulate NMDARs simultaneously via the two pathways, Homer- and G-protein-controlled. The pathway which prevails is dependent on the time scale of activation: the fast Homer-transduced effect is more prominent at short-term intervals after mGluRIs activation, whereas the slower, G-protein-delivered effect has an advantage on long-term intervals. To test the hypothesis, we set out to investigate the mGluRI-NMDAR interaction in two distinct cell types, where earlier studies demonstrated different long-term effects of mGluRIs on NMDAR response: potentiation (in hippocampal dentate gyrus granule cells, DGCs) (Naie and Manahan-Vaughan, 2004) and suppression (in CGCs) (Bertaso et al., 2010).

Methods and materials

Generation of cell cultures

Obtaining cells. Cultures were generated from E17.5, C57BL6-J mice. Pregnant mother was sacrificed with cervical dislocation according to UK Animals (Scientific Procedures) Act 1986 Schedule 1. Embryos were removed by caesarean section and decapitated in Hanks Balanced Salt Solution (Gibco, 14170-88) containing 5% penicillin-streptomycin (Gibco, 15070-063) on ice. Skulls were removed and brain tissue dissected under a light microscope where the cerebellum were separated followed by hippocampi removal from the embryo forebrain. Tissue was then exposed to enzymatic digestion using Papain (Worthington, LK003176) following mechanical dissociation in complete DMEM (Gibco, 11960-044) containing 10% Fetal Bovine Serum (Gibco, 10500) and 5% penicillin-streptomycin. Tissue was washed with DMEM and pelleted twice before being resuspended in complete Neurobasal media (Gibco, 21103049) containing 10% B27 (Gibco, 17504), 5% PenStrep and 0.25% L-gluatamine (Gibco, 25030). Cells were plated at a density of 2-5x10^4 cells/ml on glass cover slips that had been coated with Poly-D-Lysine (Sigma, P7280) and Laminin protein (Gibco, 2301015). Cultures were maintained in a humidified incubator at 37 $^{\circ}$C, under 5% CO_2.

Transfection. Granule cells were transfected at *DIV7* with pRK5-Homer1a overexpression vector and mCherry fluorescent marker vector (Clontech, 632523) using Lipofectamine 2000 (Thermo, 11668027). 250ng DNA per vector was added to Optimem then incubated with

Lipofectamine at room temperature before being dripped onto the cultures and left to recover for 5 days before recording were taken.

Electrophysiology

Visualized patch-clamp recordings from cultured granule cells were performed using an infrared differential interference contrast imaging system. The perfusion solution contained the following (in mM): 119 NaCl, 2.5 KCl, 1.3 Na_2SO_4, 2.5 $CaCl_2$, 26.2 $NaHCO_3$, 1 NaH_2PO_4, 22 glucose and was continuously gassed with 95%O_2 and 5%CO_2, pH 7.35; 290–298 mOsm. The intracellular pipette solution for voltage-clamp experiments contained (in mM): 120.5 CsCl, 10 KOH-HEPES, 2 EGTA, 8 NaCl, 5 QX-314 Br^- salt, 2 Na-ATP, 0.3 Na-GTP. For current-clamp recordings intracellular pipette solution contained (in mM): 126 K-gluconate, 4 NaCl, 5 HEPES, 15 glucose, 1 K_2SO_4·7H2O, 2 BAPTA, 3 Na-ATP. pH was adjusted to 7.2 and osmolarity adjusted to 295 mOsm.

In experiments on DGCs we selected for patching neurons which morphology reproducing that reported for mature DGCs in culture: cells with roundish body of 10-15 μm and bipolar neurites (Lowenstein and Arsenault, 1996). Each patched cell was first tested for electrophysiological properties. Further experimental procedures were performed at cells reproducing all three characteristics of mature DGCs: whole-cell capacitance of 15-25 pF, membrane potential of -65-75 mV, input resistance of 150-300 MΩ (Spampanato et al., 2012).

In experiments on CGC we selected for patching cells with mature morphology reproducing that observed in our earlier study: small (~5 μm) neurons with short dendrites (Sylantyev et al., 2013), and then monitored their electrophysiological properties. We continued experimental protocol on cells reproducing all three of the following characteristics: whole cell capacitance of 2-5 pF, membrane potential -60-70 mV, input resistance 5-8 GΩ (Hevers and Luddens, 2002; Sylantyev et al., 2013).

Outside-out and nucleated patch recordings. Outside-out patches (OOPs) and cell membrane bags containing intact nucleus and cytoplasm (nucleated patches, NPs) were pulled from dentate gyrus granule cells and cerebellar granule cells, and recordings were performed in voltage-clamp mode (V_{hold} -70 mV). Solution exchange experiments were performed as described in our earlier published protocol (Sylantyev and Rusakov, 2013). Briefly, we used a θ-glass application pipette with ~200 μm tip diameter attached to the micromanipulator. The position of the pipette was controlled by piezoelectric element (the speed of switch was 50–100μs). One pipette channel was filled with the bath aCSF solution; another channel had glutamate receptors ligands. Pressure was regulated by a PDES-02DX pneumatic micro ejector (npi) using compressed nitrogen separately in each of two channels. Solutions with NMDA + Glycine, NMDA + Glycine +

DHPG and NMDA + Glycine + FTIDC + Fenobam were exchanged in a pipette channel (7–12 s) during the exposure of nucleated patch to the bath solution channel.

Whole-cell recordings. Whole-cell EPSPs were measured in current-clamp mode in the presence of the following set of ligands: picrotoxin (50 μM), NBQX (20 μM), strychnine (1 μM), CGP-55845 (1 μM). Recordings were performed at 32-34°C; the patch pipette resistance was 3-7 MΩ depending on particular experimental conditions. Series resistance was monitored throughout experiments using a +5 mV step command, cells with unstable series resistance (above 25 MΩ) or unstable holding current were rejected.

To assess modulation of synaptic efficacy in polysynaptic signalling pathways we used experimental approach tested on hippocampal cell cultures earlier (Bi and Poo, 1999). Briefly, evoked postsynaptic currents (EPSCs) were recorded from the neuron in a network of 20-30 cells (cut from surrounding cell culture by blunt electrode) after current injection applied to another patched neuron nearby. For the sake of clarity, we isolated segments of neuronal networks containing only one Homer1a-overexpressing cell, which was recorded when disruption of Homer interlink was studied; or no Homer1a-overexpressing cells when we studied G-protein-delivered crosstalk. Perfusion solution in this experiment did not contain receptor antagonists. Each EPSC component propagated by recorded neuron was interpreted as a signal delivered through separate polysynaptic pathway with a specific transmission delay. To quantify the impact of mGluRI-NMDAR crosstalk on synaptic efficacy, we measured probability of EPSC components occurrence (*P*) in control and after series of paired stimuli, when G-protein signalling cascade and/or Homer protein interlink were interrupted. To allow registration of both increase and decrease of *P*, in the beginning of experiment stimulation was adjusted to generate *P* in an interval 25%<*P*<75%. If under control conditions EPSC component had *P* out of this interval, the component was not used in further statistical calculations.

Fluorescent imaging and immunostaining

DIV11-14 mCherry-positive cells were selected for tests of Homer1a-overexpression effects using induced fluorescence (λ_{em} 580 nm). Experimental test of calbindin-D_{28k} presence was done with a method described earlier (Müller et al., 2005). To do this, whole-cell patch-clamp was performed with the green fluorescent protein (GFP) added to intracellular solution. After patching and recording of electrophysiological parameters (membrane potential, membrane capacitance, input resistance) patching pipette was withdrawn and a fluorescent image of the patched cell taken (λ_{em} 510 nm). Hereupon coverslips were placed to 4% paraformaldehyde for 12 h at room temperature and then incubated at 4°C for 24 h with monoclonal mouse anti-calbindin-D_{28k} antibodies (1:1000) in TBS with 0.3% Triton X-100. Next, biotin-conjugated sheep anti-mouse antibodies (1:200) and streptavidin-conjugated Cy5 (1:300) were applied sequentially overnight; then Cy5 fluorescence imaged (λ_{em} 670 nm).

Acquisition and analysis

Recordings were obtained using a Multi-Clamp 700B amplifier (Molecular Devices), filtered at 4-8 kHz, digitized at 10 kHz, and stored on a PC. pClamp/Clampfit 10x software (Molecular Devices) was used for data storage and off-line analysis.

Analysis of the macroscopic currents. Activation of NMDA receptors with high concentrations of NMDA and glycine (50 μM each) at outside-out and nucleated patches evoked macroscopic responses, where "peak response" was obtained as a difference between baseline (average for 50 ms before application of NMDA receptor ligands) and maximum evoked current; "stable" or "equilibrated" response was obtained as a difference between baseline and stable current generated at 200-800 ms interval ~4 s after start of continuous application of NMDA receptor ligands.

Analysis of the single-channel recordings. Activation of NMDA receptors with low concentration of NMDA and glycine (1 μM each) at outside-out and nucleated patches evoked single-channel openings to three conductance levels: 51.9 ± 7.8 pS, 37.2 ± 6.4 pS and 22.1 ± 8.3 pS. The larger conductance level contributed 91.9% of the single channel current whereas medium and low subconductance levels contributed 6.2% and 1.9% of the current, respectively; thus the larger main conductance level was used when (possible) changes of single-channel conductance were compared under different experimental conditions. Because it was virtually impossible to determine accurately the number of channels in a nucleated patch, the open probability was obtained as the total open probability of N channels (NP_o), calculated as the proportion of the channel total open time to the duration of recording. Since NP_o in individual patches widely varied (from 0.02 to 0.2), for statistical calculations we used values normalized to control (NP_o generated by NMDA+Gly in corresponding patch). With the low (1 μM) NMDA and glycine concentrations used in this study, the majority of channel events were single level events. In a case where there were multiple levels of channel openings, only level with highest conductance was analysed. This prevented us from overestimation of NP_o increase, since in multi-channel patch increased NP_o would be accompanied by increase of proportion of multi-level events. To inspect the stationarity of channel activities, conductance, NP_o and the open time were followed in control experiments for up to 15 min; no time-dependent alterations were detected.

Strychnine, FTIDC, Fenobam, GGP-55845, NBQX, APV and pertussis toxin were purchased from Tocris Bioscience. All other chemicals, biotin-conjugated sheep anti-mouse antibodies and monoclonal anti-calbindin-D_{28k} mouse antibodies were purchased form Sigma-Aldrich. Streptavidin-conjugated Cy5 and GFP were purchased from ThermoFisher.

All data is given as Mean ± Standard Error of Mean. Statistical comparisons were made with Student's unpaired t-test, unless different is indicated in the text; P-value of ≤0.05 was taken as a threshold of significance.

Figures 9E and 10 were created with elements from Motifolio PPT Neuroscience Toolkit 2010.

Results

mGluRIs modulate equilibrated NMDAR response. First, we tested mGluRI-NMDAR interaction on nucleated membrane patches where solutions containing mGluRI and NMDAR ligands were exchanged on the same patch, with registration of stable response amplitude. Three combinations of ligands were applied at the same patch sequentially. First, 50 μM NMDA + 50 μM glycine (Gly) to activate only NMDARs. Second, 50 μM NMDA + 50 μM Gly + 50μM DHPG to activate NMDARs and mGluRIs; being compared to response generated by NMDARs only, this should reveal mGluRIs modulatory effect on NMDARs. Third, 50 μM NMDA + 50 μM Gly + inverse agonists of mGluRIs: 100 nM FTIDC and 1 μM Fenobam (FB); comparison to "NMDARs only" response should reveal whether mGluRIs modulate NMDARs due to spontaneous activation. Each solution was applied for four seconds, as this time was enough to stabilise NMDAR response amplitude. This protocol was repeated on intact cells and cells overexpressing Homer1a with standard intracellular solution and intracellular solution containing PeTX (1 μg/ml), which allowed us to register four modes of mGluRI-NMDAR crosstalk: (i) intact cell, standard internal solution: both Homer- and G-protein signalling pathways are active; (ii) intact cell, internal solution with PeTX: only Homer signalling pathway is active; (iii) Homer1a overexpressing cell, standard internal solution: only G-protein signalling pathway is active; (iv) Homer1a overexpressing cell, internal solution with PeTX: both signalling pathways are blocked. To account for individual patch characteristics, for statistical calculations the response amplitudes were normalised to the amplitude of response generated by the application of 50 μM NMDA + 50 μM Gly.

Nucleated patches from DGCs, subjected to this experimental protocol, demonstrated a significant impact of mGluRIs on NMDAR function delivered through both Homer- and G-protein signalling chains. In contrast, the application of mGluRI inverse agonists, as in all further experiments, did not cause any significant modulation of effect generated by NMDA+Gly (Fig. 1). Normalised response amplitude, (i): 1.29 ± 0.094 when mGluRIs were activated by DHPG vs. 0.95 ± 0.155 when mGluRIs were blocked by FTIDC+FB; (ii): 1.19 ± 0.068 vs. 1.03 ± 0.12; (iii): 1.66 ± 0.13 vs. 1.02 ± 0.1; (iv): 1.04 ± 0.11 vs. 1.01 ± 0.13. Significance of difference from unity, when mGluRIs were activated: for (i) $P = 0.036$, $n = 9$; for (ii) $P = 0.034$, $n = 6$; for (iii) $P = 0.004$, $n = 6$, paired Student's t-test. The normalised mGluRIs-modulated response in mode (iii) was also significantly higher than that of type (i): 1.66 ± 0.13 vs. 1.3 ± 0.094, $P = 0.044$, $n = 6, 9$, Student's t-test (Fig. 1C).

When a similar experiment was repeated on nucleated patches from CGCs (Fig. 2), only G-protein signalling pathway, being activated alone (mode (iii)), generated a significant modulatory

(downregulatory) effect. Normalised response amplitude, (i): 1.06 ± 0.07 when mGluRIs were activated vs. 0.92 ± 0.07 when mGluRIs were blocked; (ii): 1.11 ± 0.08 vs. 1.05 ± 0.06; (iii): 0.66 ± 0.05 vs. 0.96 ± 0.08; (iv): 1.00 ± 0.09 vs. 0.97 ± 0.07. Significance of difference from unity when mGluRIs were activated for (iii): P = 0.016, n = 6, paired Student's t-test; in all other cases no significant difference was observed (Fig. 2C)

As a control, we tested this experimental protocol on outside-out patches excised from DGCs and CGCs, where both Homer- and G-protein signalling chains were supposed to be destroyed. As expected, in this experiment any kind of pharmacological manipulations did not exert any significant effect (Fig. 3).

mGluRIs modulate single-channel opening probability of NMDARs. After studying mGluRIs' impact on macroscopic NMDAR response, we asked how mGluRIs modulate the functional characteristics of individual NMDAR ion channels. To clarify this, we repeated the same experimental protocol, but with lowered concentrations of NMDA (1 μM) and Gly (1 μM) to make single-channel openings visible. Channel conductance, average open time, and opening probability were used as quantitative characteristics of mGluRIs effect (Fig. 4).

In DGCs, the average open time (13.7 ± 2.6 ms) and single-channel conductance (52.1 ± 2.4 pS) were indistinguishable between recordings in modes (i) - (iv) (Fig. 4C). However, data on opening probability demonstrated a significant upregulation of NMDAR function in (i), (ii), and (iii) modes, when normalised to control. (i): 1.52 ± 0.13 when mGluRIs were activated vs. 1.12 ± 0.11 when mGluRIs were blocked; (ii): 1.26 ± 0.1 vs. 1.03 ± 0.03; (iii): 1.65 ± 0.2 vs. 1.06 ± 0.11; (iv): 1.01 ± 0.07 vs. 0.95 ± 0.15. Significance of difference from unity when mGluRIs were activated for (i), (ii) and (iii): P = 0.002, 0.029, 0.013, respectively, n = 6 for all cases, Student's t-test. In mode (iv) no significant difference from unity was observed (Fig. 4C).

In CGCs, similar to DGCs, the disruption of G-protein- and Homer-containing mGluRI-NMDAR crosstalk did not result in significant changes of average open time (11.9 ± 3.2 ms) and single-channel conductance (51.6 ± 3.7 pS) (Fig. 5). However, in CGCs experimental modes (ii) and (iii) showed a significant mGluRIs effect on opening probability (Fig. 5C). (i): 1.1 ± 0.15 when mGluRIs were activated vs. 1.07 ± 0.1 when mGluRIs were blocked; (ii): 1.31 ± 0.18 vs. 1.23 ± 0.19; (iii): 0.83 ± 0.06 vs. 0.93 ± 0.1; (iv): 0.93 ± 0.06 vs. 0.96 ± 0.12. Significance of difference from unity when mGluRIs were activated for (ii) and (iii): P = 0.042 and 0.037, respectively, n = 6 for both cases, Student's t-test.

Rapid potentiation of NMDAR effect is delivered exclusively through Homer-containing interlink. After experiments on long intervals, where Homer- and G-protein-delivered effects overlapped, we tested mGluRI-NMDAR modulation at short intervals (units of milliseconds). We

presumed that, under these conditions, the G-protein-delivered effects might not have enough time to fully develop, as was observed earlier (Sylantyev et al., 2013).

We found in both DGCs and CGCs that after rapid (~1 ms) application of agonists, the activation of mGluRIs has increased peak amplitudes of NMDAR response independently of PeTX presence in the internal solution. For DGCs (Fig. 6), (i): DHPG in applied solution increased the response amplitude by 16.09 ± 1.48% vs. 0.68 ± 1.75% when the applied solution contained FTIDC+FB; (ii): 12.52 ± 1.42% vs. -0.1 ± 1.74%. For (i) and (ii) significance of difference from zero when mGluRIs were activated: P = 0.003 and 0.004, respectively, n = 6. However, Homer1a overexpression prevented such a potentiation. (iii): 3.68 ± 2.01% vs. 1.87 ± 2.54%; (iv): 1.54 ± 1.94% vs. -0.02 ± 1.66%; P>0.05 for both cases, n=6 (Fig. 6C). The same experiment on CGCs (Fig. 7), (i): 9.88 ± 1.5% vs. 3.2 ± 2.18%; (ii): 9.57 ± 1.93% vs. 0.97 ± 2.78%; (iii): 2.15 ± 2.49% vs. 1.76 ± 1.77%; (iv): 1.97 ± 2.15% vs. 2.3 ± 2.12%. Significance of difference from zero when mGluRIs were activated in intact cells ((i) and (ii)): P = 0.006 and 0.008, respectively, n = 6 for both cases, paired Student's t-test (Fig. 7C). In all recordings, the maximum potentiation effect of mGluRIs developed within the 5 ms time window after the application of ligands (Fig. 6 and 7).

mGluRIs modulate NMDAR-generated action potentials via both Homer- and G-proteins signalling pathway. Next, we asked whether, and to what extent Homer- and G-protein-mediated mGluRI-NMDAR signalling pathways regulate the generation of neuronal action potentials (APs). To clarify this, we performed whole-cell recordings from neurons in dispersed cell culture, where APs were evoked by consequent 300 ms applications of the same set of solutions, as in the experiments on membrane patches (Fig. 8). To quantify mGluRIs input into AP generation, we used action potential ratio (APR) obtained as a number of APs evoked when NMDARs and mGluRIs are activated with DHPG+NMDA+Gly or mGluRIs are suppressed with NMDA+Gly+FTIDC+FB, divided by number of APs generated in the same cell by NMDA+Gly only.

Here we found that in DGCs blocking of each signalling pathway leads to a significant reduction of APR compared to control value. (i), control: 1.82 ± 0.19 when mGluRIs were activated vs. 1.08 ± 0.14 when mGluRIs were blocked, (ii): 1.32 ± 0.1 vs. 1.04 ± 0.13, (iii): 1.52 ± 0.09 vs. 1.1 ± 0.11; (iv): 1.17 ± 0.18 vs. 1.02 ± 0.12. Significance of difference from control when mGluRIs were activated in modes (ii), (iii) and (iv): P = 0.044, 0.047 and 0.032, respectively, n = 6 for all three comparisons, paired Student's t-test. When Homer- and G-protein pathways were blocked simultaneously in (iv), the firing frequency observed with DHPG and FTIDC+FB in the applied solution became indistinguishable from unity (i.e. from that generated by NMDA+Gly only): P = 0.144 and 0.426 for DHPG and FTIDC+FB, respectively, n = 6, paired Student's t-test for both APR comparisons (Fig. 8E).

In contrast, in CGCs only Homer1a overexpression triggered significant mGluRIs-mediated modulatory effects on APR when compared to control. (i), control: 1.15 ± 0.17 when mGluRIs were activated vs. 0.92 ± 0.13 when mGluRIs were blocked; (ii): 1.47 ± 0.14 vs. 1.08 ± 0.12; (iii): 0.81 ± 0.08 vs. 0.95 ± 0.14; (iv), 1.05 ± 0.11 vs 1.16 ± 0.14. APR in (iii) was significantly lower when compared to control and to unity: P = 0.042 and 0.021, respectively, n = 8 for both comparisons, paired Student's t-test. As in DGCs, under mode (iv) APR generated with DHPG and FTIDC+FB was indistinguishable from unity: P = 0.35 and 0.08, respectively,, n = 6, paired Student's t-test for both comparisons (Fig 8F).

mGluRI-NMDAR crosstalk modulates synaptic plasticity.

As the next step, we set out to clarify the role of two types of mGluRI-NMDAR crosstalk in synaptic transmission and induction of synaptic plasticity. To comprehend this, we used networks of cultured neurons where two polysynaptically connected cells were patched simultaneously. Current injection into one cell (held in current-clamp mode) generated action potential with the subsequent poly-component EPSC recorded from another cell (held in voltage-clamp mode). We interpreted each EPSC component as a signal through separate transmission pathway with specific delay. Under the low-frequency stimulation (1 current injection per 15 seconds) the probability of occurrence (*P*) remained stable for each EPSC component observed in recorded cell. We thus used the EPSC profile as a tool for quantitative measurement of synaptic efficacy (see Methods for more details). To examine synaptic plasticity in recorded network, we applied a train of 50 paired-pulse stimuli with 50 ms inter-pulse interval at 1Hz. After that, we monitored changes in *P* (decrease or increase, i.e. ΔP) of pre-existing EPSC components, which reflect remodelling of signalling pathways (Fig. 9A and B). Recorded neurons held in mode (i)-(iv) allowed assessment of the input of two types of mGluRI-NMDAR crosstalk into modulation of synaptic plasticity.

We found, that in DGCs blocking of each mGluRI-NMDAR crosstalk pathway induces a significant lowering of ΔP. (i), control: 0.24 ± 0.023 when mGluRIs were activated vs. 0.15 ± 0.019 when mGluRIs were blocked; (ii): 0.17 ± 0.022 vs. 0.12 ± 0.015; (iii): 0.16 ± 0.017 vs. 0.1 ± 0.013; (iv): 0.14 ± 0.021 vs. 0.13 ± 0.018. Significance of difference from control for (ii)-(iv): P = 0.038, 0.022, 0.034, respectively, n=7, Student's t-test. In modes (i)-(iii) block of mGluRIs caused significant reduction of ΔP compared to readout when mGluRIs were active in the same mode: P = 0.021, 0.031, 0.036, respectively, n=7, Student's t-test for all three comparisons (Fig. 9C).

In turn, in CGCs blocking of Homer pathway (mode (iii)) did not trigger significant change of ΔP when compared to control, unlike the block of G-proteins chains (ii) and of both signalling pathways (iv). (i), control: 0.26 ± 0.013 when mGluRIs were activated vs. 0.18 ± 0.03 when mGluRIs were blocked; (ii): 0.19 ± 0.011 vs. 0.14 ± 0.013; (iii): 0.21 ± 0.013 vs. 0.16 ± 0.02; (iv):

0.12 ± 0.022 vs. 0.12 ± 0.02. For comparisons of (ii) and (iv) to control when mGluRIs activated P = 0.0102 and 0.011, respectively, n=8, Student's t-test. As in DGCs, in modes (i)-(iii) block of mGluRIs caused significant reduction of ΔP compared to readout when mGluRIs were active: P = 0.018, 0.045 and 0.019, respectively, n=8, Student's t-test for all three comparisons (Fig. 9C).

For both DGCs and CGCs we did not observe significant difference of ΔP values obtained when mGluRIs were blocked under any experimental mode ((i)-(iv)), from ΔP obtained when mGluRIs were activated, but both mGluRI-NMDAR signalling pathways were blocked (iv): P>0.05 for all comparisons, n=7 (DGCs) and n=8 (CGCs), Student's t-test (Fig. 9C).

As a general rule, alterations of post-synaptic current profile displayed changes in *P* of particular components, but without substantial variation of their amplitude. In DGCs under mode (i) amplitude of the first peak after the stimulation train was changed by +17±22% when compared to pre-train value, under mode (ii) by -11±19%, under mode (iii) by +21±18%, under mode (iv) by +7±16%; P>0.3 for all comparisons to pre-train value, n=7, Student's t-test. In CGCs under mode (i) first peak amplitude was changed by +14±9%, under mode (ii) by -8±13%, under mode (iii) by -4±11%, under mode (iv) by +9±8%; P>0.2 for all comparisons to pre-train values, n=8, Student's t-test.

Next, to quantify the role of NMDARs in synaptic plasticity and signaling pathways remodeling, we repeated the same experimental protocol, but with pharmacological block of NMDARs (with 50 μM APV) rather than of mGluRIs. We found, that pharmacological silencing of NMDARs induces a significant decrease of ΔP values, i.e. much fewer changes of EPSC profiles were observed under all experimental modes (Fig. 9D). For DGCs, mode (i): 0.075±0.023 when NMDARs were blocked vs. 0.23±0.033 when NMDARs were active; mode (ii): 0.067±0.018 vs. 0.16±0.039; mode (iii): 0.049±0.02 vs. 0.18±0.022; mode (iv): 0.035±0.014 vs. 0.11±0.014. For comparisons "APV - active NMDARs" P=0.0032, 0.0067, 0.0054 and 0.0086 for modes (i), (ii), (iii) and (iv), respectively, n=7, Student's t-test. For CGCs, mode (i): 0.058±0.02 when NMDARs were blocked vs. 0.24±0.42 when NMDARs were active; mode (ii): 0.61±0.022 vs. 0.17±0.021; mode (iii): 0.048±0.011 vs. 0.15±0.019; mode (iv): 0.046±0.011 vs. 0.09±0.024. For comparisons "APV – active NMDARs" P=0.0028, 0.0073, 0.0062 and 0.023 for modes (i), (ii), (iii) and (iv), respectively, n=7, Student's paired t-test.

Finally, as an additional control, we tested accuracy of our cell selection algorithm on DGCs (Fig. 9F and G). To do this, we patched cultured cells, pre-selected on visual criteria, with pipette solution containing GFP. If cell electrophysiological parameters were in pre-defined intervals (membrane capacitance 15-25 pF, membrane potential -65-75 mV, input resistance 150-300 MΩ), we performed an accurate withdrawal of patch pipette and captured an image of GFP fluorescence. Afterwards, the coverslip with cell culture underwent immunostaining with Cy5

fluorescent dye for the protein calbindin-D_{28k} which is a characteristic DGC marker (Müller et al., 2005); see Methods for more details.

All six cells which reproduced pre-defined electrophysiological parameters, have also demonstrated Cy5 fluorescence, thus confirming that chosen selection algorithm circumscribes at least a part of DGCs population. Electrophysiological readouts in this experiment were as following: membrane capacitance 21.61±2.77 pF; membrane potential 68.25±3.12 mV; input resistance 271.92±9.33 MΩ.

Discussion

In this work we examined the mGluRI-NMDAR crosstalk through two pathways: G-protein-mediated and Homer-mediated (Fig. 10). At a short time interval (units of milliseconds) the only significant result of such a crosstalk, similar for DGCs and CGCs, was a facilitation of NMDAR response triggered by mGluRIs and delivered through Homer-containing scaffold. On a long time interval (from hundreds of milliseconds to seconds) this facilitation overlaps with slower modulatory impact delivered through G-protein-initiated signalling cascade. Type of G-protein-delivered impact (facilitation or depression) depends on the particular cell type. Form of the end result of mGluRI-NMDAR crosstalk is therefore cell-specific and depends on a registration timescale.

In DGCs the mGluRIs generated a significant potentiation of long, equilibrated NMDAR response under control conditions (Fig. 1) in line with earlier reports (Awad et al., 2000). The potentiation generated by mGluRIs in Homer1a-overexpressing DGCs, i.e. delivered through G-protein pathway only, was significantly higher than that delivered via both G-protein and Homer pathway in intact cells (Fig 1C). This implies the competitive nature of the two, albeit unidirectional, signals. In contrast, in CGCs only the G-protein pathway, being activated alone in Homer1a overexpressing cells, induced a significant downregulation of NMDAR effect, thus resembling earlier observations (Bertaso et al., 2010). No significant effect of any direction was generated by the Homer pathway only, or when both pathways were active (Fig. 2). The plausible explanation is that, the readout of the Homer-delivered effect on equilibrated response in CGCs is below the applied method's sensitivity, but this pathway functionally prevails over G-protein signalling, and thus muffles the downregulation delivered through G-proteins.

For both DGCs and CGCs no significant effect of mGluRIs was demonstrated when Homer- and G-protein-controlled pathways were simultaneously blocked (Fig. 1C, 2C), which implies the lack of significant input from other mechanisms of mGluRI-NMDAR crosstalk. Next, we observed the effect of DHPG in nucleated patches (Fig. 1, 2, 4–7) and in whole-cell (Fig. 8, 9), but not in

outside-out patches (Fig. 3). This proves the critical dependence of mGluRI-NMDAR interaction from cytoplasmic elements and/or elements not anchored into outer cell membrane. On top of that, the lack of DHPG effect in outside-out patches proves that DHPG does not activate NMDARs directly, acting as NMDA co-agonist (Contractor et al., 1998).

An alternative pathway of mGluRI-NMDAR crosstalk is modulation of assembly of Homer-containing protein scaffold, where repetitive NMDAR activation shifts equilibrium to disassembled state (Moutin et al., 2012); (see Fig. 10). Can this pathway be involved into modulation of effects studied in our research? Moutin and co-authors demonstrated localization of such a process exclusively in post-synaptic compartments, thus it could exert an effect in whole-cell experiment (Fig. 9). In contrast, axo-somatic synapses were reported for DGCs (Toni et al., 2007), however, to the best of our knowledge, not for CGCs. Therefore, similar results of Homer-delivered rapid effects obtained after repetitive NMDAR activation on NPs pulled from both DGCs and CGCs (Fig. 6, 7) argue against presence of NMDAR-induced disruption of Homer-containing interlink at least in this type of experiments.

In contrast to the equilibrated NMDAR response (Fig. 1, 2), where the effect of mGluRIs was specific to the cell type under study (potentiation of NMDAR response in DGCs, suppression in CGCs), at a short time interval after rapid ligand application, the mGluRIs potentiate an NMDAR response amplitude in both cell types (Fig. 6, 7), resembling short-term mGluRI effects which have been documented earlier (Kinney and Slater, 1993; Rossi et al., 1996; Sylantyev et al., 2013). This potentiation is insensitive to PeTX, but does not develop in Homer1a overexpressing cells, thus suggesting the Homer protein chain as the only underlying mechanism.

Despite of apparent modulatory impact of mGluRI-NMDAR crosstalk on neural signalling revealed in our experiments, it is still an important question: whether our data represent a typical set of effects? Or this is a result of specific combination of experimental conditions, such as the age of tested cells and extrasynaptic, rather than synaptic, localization of recorded receptors in experiments on membrane patches? It was reported earlier that synaptic and extrasynaptic pools of NMDARs display different proportions of NR1 and NR2 subunits (Barria, 2007), whereas different receptor subunits interact differently with PSD-95 protein (Patrick et al., 1999; Al-Hallaq et al., 2007), which links them to mGluRI via the Homer-containing scaffold (Fig. 10). On top of that, expression levels of different NMDAR subunits (Monyer et al., 1994) and different types of Homer protein (Shiraishi et al., 2004) are age-dependent. However, it was shown that NMDARs and Homer proteins make functional clusters throughout all developmental stages both in extrasynaptic and synaptic loci of cultured neurons (Shiraishi et al., 2003). Apart of that, studies on cultured neurons of different age demonstrated effects of mGluRI-Homer-NMDAR interaction similar to our present observations. These effects were found in CGC NPs (Sylantyev et al., 2013), i.e. were generated by extrasynaptic receptors, and in a whole cell (Bertaso et al., 2010),

i.e. were generated primarily by synaptic receptors. Similarly, G-protein-mediated mGluRI-NMDAR modulation was demonstrated in cultured neurons from earliest stages of their development (Hilton et al., 2006) to maturation (Lea et al., 2002); such a modulation occurs both in synapses (Kwon and Castillo, 2008) and at extrasynaptic membrane (our data). These observations suggest that mGluRI-NMDAR signaling pathways researched in our study preserve their functionality independently from particular receptors localization and the cell age. However, their relative input into integrated modulatory tone may vary depending on a stage of the neuron development.

NMDARs are widely recognized to play a pivotal role in long-term synaptic plasticity in the central nervous system (Malenka and Nicoll, 1993; Paoletti et al., 2013). In our work we demonstrated two mGluRI-NMDAR crosstalk pathways to be modulators of ΔP, i.e. of NMDARs input into changes of synaptic strength after series of paired stimuli (Fig. 9D). Therefore, we found that G-protein-controlled and Homer-controlled signalling pathways between mGluRI and NMDAR play a significant role in synaptic plasticity and efficacy.

Our further experiment on the signalling pathways remodelling demonstrated that NMDARs silencing with APV reduces significantly variability of neural network synaptic transmission and synaptic strength (ΔP), which is consistent with earlier observations of involvement of synaptic NMDARs into long-term plasticity (Bi and Poo, 1999; O'Riordan et al., 2018). However, even when both mGluRI-NMDAR signalling pathways were blocked (mode (iv)) and APV added, we did observe certain degree of ΔP (Fig. 9D and E). This may reflect involvement of mGluRI- and NMDAR-independent mechanisms such as modification of GABA-ergic conductance (Linden and Connor, 1995) and/or activity-dependent modifications of neuronal excitability (Turrigiano et al., 1994).

Our experiments on neural networks demonstrated that similar pattern of stimuli can induce opposite changes along different signaling pathways (increase or decrease of P). Modulation of EPSC profiles without significant impact on response amplitudes suggests that the chosen pattern of stimulation had caused variation of synaptic strength at remote synaptic connections, thus changing the probability of a signal transmission by different pathways connecting stimulated and recorded cell, with variable interplay between these pathways. This type of modification is consistent with a paradigm of distributed storage and representation of information in neural networks (Churchland and Sejnowski, 1992; Bliss and Collingridge, 1993).

Constitutive agonist-independent activity of G-protein-coupled receptors was repeatedly detected in various experimental setups and may substantially impact cell functioning and intercellular signalling (Milligan, 2003). However, the absence of any detectable difference between mGluRI effects under control and when mGluRI inverse agonists FTIDC and FB are

applied in all types of experiments, suggests that NMDAR effects triggered by NMDA+Gly alone (i.e. without activation of mGluRIs) are not modulated by spontaneous mGluRIs activity. Thus, we presume that the non-significant effects of mGluRIs activation in intact CGCs (Fig. 8F) is due to the overlap of Homer- and G-protein-delivered signals of opposite sign, rather than the result of say the majority of mGluRIs in the active state (due to spontaneous activation) before application of DHPG.

Therefore, in our study we found the functional mechanism of mGluRI-NMDAR interaction in DGCs and CGCs to be as follows (Fig. 10): mGluRIs, when activated, modulate NMDARs simultaneously through Homer- and G-protein-controlled pathways via changes of NMDAR opening probability. The Homer-containing protein interlink delivers potentiating signal to NMDARs in both cell types, whereas the G-protein-mediated signal is cell-specific: it potentiates NMDAR function in DGCs and suppresses it in CGCs. Fast Homer-transduced effect is more prominent at short time intervals after mGluRIs activation, whereas slower developing G-protein-delivered effect has an advantage on long-term intervals. Additionally, Homer-mediated potentiation tone prevails over modulation delivered by G-proteins cascade, although it causes smaller absolute effect.

The hippocampus has been recognised as a key brain area in schizophrenia development (Harrison, 2004), associated with decreased NMDAR function (Gao et al., 2000). Here we observed an increase of NMDAR conductivity in Homer1a overexpressing DGCs (Fig. 1C) due to higher mGluRI-triggered potentiation delivered through a G-protein chain, rather than through a competing Homer interlink (see Fig. 1C, 4C, 8E). This suggests a plausible mechanistic explanation for haloperidol and clozapine's anti-schizophrenia effects associated with the upregulation of Homer1a synthesis (Polese et al., 2002).

Figure legends

Figure 1. mGluRIs potentiate amplitude of equilibrated NMDAR response through G-protein and Homer signalling pathways in DGCs. A: Nucleated patches excised from control cell. Left: standard intracellular solution (both signalling pathways are active). Right: PeTX added to intracellular solution (only Homer pathway active). **B:** Nucleated patch excised from the Homer1a overexpressing cell. Left: standard intracellular solution (only G-protein signalling pathway active). Right: PeTX added to intracellular solution (both signalling pathways are blocked). Colour codes of applied ligand cocktails and scale bars apply to A and B. Dashed line marks time interval where response amplitude was calculated. **C:** Statistical summary of A and B. Response amplitudes are normalized to amplitude generated by NMDA+Gly. Asterisks above bars denote significance of difference from unity. * - P<0.05, ** - P<0.01, Student's t-test. Inset: fluorescent image of cultured DGC co-transfected with Homer1a and mCherry.

Figure 2. mGluRIs downregulate amplitude of equilibrated NMDAR response through G-protein signalling pathway in CGCs. A: Nucleated patch excised from control cell. Left: standard intracellular solution. Right: PeTX added to intracellular solution. **B:** Nucleated patch excised from the Homer1a overexpressing cell. Left: standard intracellular solution. Right: PeTX added to intracellular solution. Colour codes of applied ligand cocktails and scale bars apply to A and B. **C:** Statistical summary of A and B. Response amplitudes are normalized to amplitude generated by NMDA+Gly. Asterisks above column denote significance of difference from unity. ** - P<0.01, paired Student's t-test. Inset: fluorescent image of cultured CGC co-transfected with Homer1a and mCherry.

Figure 3. mGluRI-NMDAR crosstalk is absent in outside-out patches. A-D: Example traces from experimental protocols where significant mGluRI effect was observed in nucleated patches (refer to Fig. 1C and 2C). A: Outside-out patch from intact DGC, standard intracellular solution. B: Outside-out patch from intact DGC, internal solution with PeTX. C: Outside-out patch from DGC overexpressing Homer1a, standard internal solution. D: Outside-out patch from intact CGC, internal solution with PeTX. Scale bars and colour codes apply to A-D. **E:** Statistical summary on normalized response amplitudes for (i), (ii), (iii) and (iv) experimental modes in DGCs and CGCs. Amplitudes normalized to the value generated by NMDA+Gly.

Figure 4. mGluRIs modulate NMDARs opening probability in DGCs. A: Control cell. **B:** Homer1a overexpressing cell. For A and B, left: standard intracellular solution; right: PeTX added to

intracellular solution. Traces from top to bottom: NMDA+Gly, NMDA+Gly+DHPG, NMDA+Gly+FTIDC+FB. Scale bars apply to A and B. **C:** Statistical summary on single-channel functional parameters for A and B. Asterisks above columns denote significance of difference from unity. * - P<0.05, ** - P<0.01, Student's t-test.

Figure 5. mGluRIs modulate NMDARs opening probability in CGCs. A: Control cell. **B:** Homer1a overexpressing cell. For A and B, left: standard intracellular solution; right: PeTX added to intracellular solution. Traces from top to bottom: NMDA+Gly, NMDA+Gly+DHPG, NMDA+Gly+FTIDC+FB. Scale bars apply to A and B. **C:** Statistical summary on single-channel functional parameters for A and B. Asterisks above columns denote significance of difference from unity. * - P<0.05, Student's t-test.

Figure 6. mGluRIs potentiate rapid NMDARs response through Homer signalling pathway only; nucleated patches excised from DGCs. A: Control cell. Left: standard intracellular solution. Right: PeTX added to intracellular solution. **B:** Homer1a overexpressing cell. Left: standard intracellular solution. Right: PeTX added to intracellular solution. Colour codes of applied ligand cocktails and scale bars apply to A and B. Each trace is an average of 3-5. ***Inset:*** Illustration of rapid solution application system (schematic) with θ-glass pipette which applies two different solutions at nucleated patch placed at a patch pipette. Numbers denote sequence of drug cocktail replacements in θ-glass pipette channels: 1 – NMDA+Gly → NMDA+Gly+DHPG; 2 – NMDA+Gly+DHPG → NMDA+Gly+FTIDC+FB. During solution replacement time periods patch was exposed to solution flowing from "bottom" channel. **C:** Statistical summary on response amplitudes in A and B. Asterisks above columns denote significance of difference from zero. ** - P<0.01, Student's t-test.

Figure 7. mGluRIs potentiate rapid NMDARs response through Homer signalling pathway only; nucleated patches excised from CGCs. A: Control cell. Left: standard intracellular solution. Right: PeTX added to intracellular solution. **B:** Homer1a overexpressing cell. Left: standard intracellular solution. Right: PeTX added to intracellular solution. Colour codes of applied ligand cocktails and scale bars apply to A and B. Each trace is an average of 3-5. **C:** Statistical summary on response amplitudes in A and B. Asterisks above columns denote significance of difference from zero. ** - P<0.01, Student's t-test.

Figure 8. G-protein- and Homer-mediated signalling chains control AP generation via NMDARs. A-D: Example recordings where AP ratio was shifted significantly from values generated by NMDA+Gly. Top: APs evoked by 300 ms application of NMDA 50 μM + Gly 50 μM. Bottom: APs evoked by application of NMDA 50 μM + Gly 50 μM + DHPG 100 μM. **A:** Intact DGC, PeTX 1 μg/ml in internal solution. **B:** Homer1a overexpressing DGC. **C:** Homer1a overexpressing DGC, PeTX in internal solution. **D:** Homer1a overexpressing CGC. Scale bars apply to A-D. **E:** Statistical summary for DGCs. Ratios of AP number generated by DHPG+NMDA+Gly to that generated by NMDA+Gly. **F:** Same as E, but for CGCs. Colour codes apply to E and F. ***Inset:*** Illustration of solution application system (schematic) with θ-glass pipette which applies solution with mGluRI and NMDAR ligands ("top" channel) at a patched neural cell. During replacement NMDA+Gly → NMDA+Gly+DHPG in "top" channel patched cell was exposed to perfusion solution flowing from "bottom" channel. Asterisks denote significance of difference from control (no PeTX added, no Homer1a overexpression). *- P<0.05, n=6-8, Student's t-test.

Figure 9. mGluRI-NMDAR crosstalk and synaptic plasticity in cultured hippocampal neurons. A, B: Traces depict 20 consecutive EPSCs (inward currents are shown upwards) recorded from a cultured neuron in response to stimulation of a nearby neuron before (A) and after repetitive paired-pulse stimulation (B). Note increase of 2nd and 3rd EPSC component numbers after paired-pulse stimulation. 20 ms scale bar apply to A and B. **C, D:** Statistical summary of pathway remodelling induced by paired-pulse stimulation with modulatory impact of mGluRIs (C) and NMDARs (D). Asterisks above "mGluRIs blocked" and "NMDARs blocked" bars denote significance of difference between responses obtained with blocked mGluRIs or NMDARs, and when both receptor species are active, under the same experimental mode. * - P<0.05, ** - P<0.01, Student's paired t-test. **E:** Sketch depicting three hypothetical polysynaptic pathways (dashed lines 1-3) leading from stimulated neuron (S) to the recorded neuron (R) with different transmission delays corresponding to the onset latencies of the three distinct EPSC components. **F:** Image series illustrating selection of DGC for further experimental work. Left column: dispersed culture, solitary DGC with developed morphology (see Methods for details). Right column: dense culture, group of differentiated DGCs. From top to bottom: images under infra-red DIC; GFP fluorescence (λ_{em} 510 nm) after whole-cell patching; Cy5 fluorescence (λ_{em} 670 nm) after immunostaining for calbindin-D_{28k}; overlap of GFP and Cy5 fluorescence patterns. Arrows point to cell soma, arrowheads point to main neurite(s), 30 μm scale bar apply to both columns. **G:** Statistical summary on electrophysiological properties of DGCs recorded in F, n=6.

Figure 10. Schematic of mGluRI-NMDAR signalling chains: Homer-mediated (white element titles) and G-protein-mediated (black element titles). Red lightning bolts designate specific points where G-protein- and Homer-mediated chain were interrupted by PeTX and Homer1a, respectively. mGluRIs and NMDARs are physically connected by scaffolding proteins of postsynaptic density, which transmit modulatory signal through scaffolding proteins in the following order: mGluRI $\rightarrow$ preso1 $\rightarrow$ Homer $\rightarrow$ SH_3 and multiple ankyrin repeat domains (Shank) $\rightarrow$ guanylate-kinase-associated protein (GKAP) $\rightarrow$ post-synaptic density 95 (PSD-95) $\rightarrow$ NMDAR. Glutamate-containing vesicles of presynaptic bouton, being exocytosed, release glutamate into synaptic cleft. Glutamate binding to mGluRI and glutamate + glycine binding to NMDAR activate both receptors. Phosphorylated NMDAR allows influx of extracellular calcium ($^{EC}Ca^{2+}$) into cell; this triggers release of intracellular calcium ($^{IC}Ca^{2+}$) from endoplasmic reticulum (ER). Activation (phosphorylation) of mGluRI, induced by glutamate binding, triggers activation of the G-protein G_q, subsequently activating phospholipase C (PLC). PLC initiates conversion of phosphoinositide (PI) to inositol 1,4,5-triphosphate (IP_3) and subsequent activation of diacylglycerol (DAG); IP_3 initiates release of intracellular Ca^{2+}. DAG, being combined with increased Ca^{2+} concentration due to NMDAR activation, causes phosphorylation of protein kinase C (PKC). PKC initiates phosphorylation of proline-rich tyrosine kinase / cell adhesion kinase β (Pyk2/CAKβ), and subsequently the cellular tyrosine kinase protein (Src). In turn, SRC potentiates NMDAR. Negative feedback loop occurs after Ca^{2+} influxed through NMDARs activates Ca^{2+}-dependant protein phosphatase 2B / calcineurin (PP2B/CaN), which dephosphorylates (i.e. at least partially deactivates) mGluRIs (Matosin and Newell, 2013).

Acknowledgements: This work was supported by the RS MacDonald Seedcorn Grant 2017 and Wellcome Trust - UoE ISSF Award to S.S. Authors thank Prof. Dmitri Rusakov (UCL) for valuable suggestions on paper preparation.

Conflict of interest: The authors declare that they have no conflict of interest.

650 **Reference list**

651 Al-Hallaq RA, Conrads TP, Veenstra TD, Wenthold RJ (2007) NMDA Di-Heteromeric Receptor Populations
652 and Associated Proteins in Rat Hippocampus. The Journal of Neuroscience 27:8334-8343.
653 Awad H, Hubert GW, Smith Y, Levey AI, Conn PJ (2000) Activation of metabotropic glutamate receptor 5
654 has direct excitatory effects and potentiates NMDA receptor currents in neurons of the
655 subthalamic nucleus. The Journal of neuroscience : the official journal of the Society for
656 Neuroscience 20:7871-7879.
657 Barria A (2007) CHAPTER 10 - Subunit-Specific NMDA Receptor Trafficking to Synapses - Bean, Andrew J.
658 In: Protein Trafficking in Neurons, pp 203-221. Burlington: Academic Press.
659 Bertaso F, Roussignol G, Worley P, Bockaert J, Fagni L, Ango F (2010) Homer1a-dependent crosstalk
660 between NMDA and metabotropic glutamate receptors in mouse neurons. PLoS One 5:e9755.
661 Bi G, Poo M (1999) Distributed synaptic modification in neural networks induced by patterned
662 stimulation. Nature 401:792-796.
663 Bliss TV, Collingridge GL (1993) A synaptic model of memory: long-term potentiation in the hippocampus.
664 Nature 361:31-39.
665 Brakeman PR, Lanahan AA, O'Brien R, Roche K, Barnes CA, Huganir RL, Worley PF (1997) Homer: a protein
666 that selectively binds metabotropic glutamate receptors. Nature 386:284-288.
667 Chowdari KV, Mirnics K, Semwal P, Wood J, Lawrence E, Bhatia T, Deshpande SN, Thelma B, Ferrell RE,
668 Middleton FA (2002) Association and linkage analyses of RGS4 polymorphisms in schizophrenia.
669 Human molecular genetics 11:1373-1380.
670 Churchland P, Sejnowski T (1992) Computational neuroscience. The computational brain. In: Cambridge,
671 MA: The MIT Press.
672 Cleva RM, Olive MF (2011) Positive allosteric modulators of type 5 metabotropic glutamate receptors
673 (mGluR5) and their therapeutic potential for the treatment of CNS disorders. Molecules 16:2097-
674 2106.
675 Contractor A, Gereau RWt, Green T, Heinemann SF (1998) Direct effects of metabotropic glutamate
676 receptor compounds on native and recombinant N-methyl-D-aspartate receptors. Proceedings of
677 the National Academy of Sciences of the United States of America 95:8969-8974.
678 Fitzjohn SM, Irving AJ, Palmer MJ, Harvey J, Lodge D, Collingridge GL (1996) Activation of group I mGluRs
679 potentiates NMDA responses in rat hippocampal slices. Neuroscience letters 203:211-213.
680 Gao XM, Sakai K, Roberts RC, Conley RR, Dean B, Tamminga CA (2000) Ionotropic glutamate receptors and
681 expression of N-methyl-D-aspartate receptor subunits in subregions of human hippocampus:
682 effects of schizophrenia. The American journal of psychiatry 157:1141-1149.
683 Harrison PJ (2004) The hippocampus in schizophrenia: a review of the neuropathological evidence and its
684 pathophysiological implications. Psychopharmacology 174:151-162.
685 Harvey J, Collingridge GL (1993) Signal transduction pathways involved in the acute potentiation of NMDA
686 responses by 1S,3R-ACPD in rat hippocampal slices. British journal of pharmacology 109:1085-
687 1090.
688 Hevers W, Luddens H (2002) Pharmacological heterogeneity of gamma-aminobutyric acid receptors
689 during development suggests distinct classes of rat cerebellar granule cells in situ.
690 Neuropharmacology 42:34-47.
691 Hilton GD, L. NJ, Linda B, M. TS, M. MM (2006) Glutamate-mediated excitotoxicity in neonatal
692 hippocampal neurons is mediated by mGluR-induced release of Ca++ from intracellular stores and
693 is prevented by estradiol. European Journal of Neuroscience 24:3008-3016.
694 Kinney GA, Slater NT (1993) Potentiation of NMDA receptor-mediated transmission in turtle cerebellar
695 granule cells by activation of metabotropic glutamate receptors. Journal of Neurophysiology
696 69:585-594.
697 Kost CK, Jr., Herzer WA, Li PJ, Jackson EK (1999) Pertussis toxin-sensitive G-proteins and regulation of
698 blood pressure in the spontaneously hypertensive rat. Clinical and experimental pharmacology &
699 physiology 26:449-455.

700 Kunishima N, Shimada Y, Tsuji Y, Sato T, Yamamoto M, Kumasaka T, Nakanishi S, Jingami H, Morikawa K
701 (2000) Structural basis of glutamate recognition by a dimeric metabotropic glutamate receptor.
702 Nature 407:971-977.
703 Kwon H-B, Castillo PE (2008) Long-Term Potentiation Selectively Expressed by NMDA Receptors at
704 Hippocampal Mossy Fiber Synapses. Neuron 57:108-120.
705 Lea PM, Custer SJ, Vicini S, Faden AI (2002) Neuronal and glial mGluR5 modulation prevents stretch-
706 induced enhancement of NMDA receptor current. Pharmacology Biochemistry and Behavior
707 73:287-298.
708 Linden DJ, Connor JA (1995) Long-term synaptic depression. Annual review of neuroscience 18:319-357.
709 Lowenstein DH, Arsenault L (1996) The effects of growth factors on the survival and differentiation of
710 cultured dentate gyrus neurons. The Journal of neuroscience : the official journal of the Society
711 for Neuroscience 16:1759-1769.
712 Malenka RC, Nicoll RA (1993) NMDA-receptor-dependent synaptic plasticity: multiple forms and
713 mechanisms. Trends Neurosci 16:521-527.
714 Matosin N, Newell KA (2013) Metabotropic glutamate receptor 5 in the pathology and treatment of
715 schizophrenia. Neuroscience and biobehavioral reviews 37:256-268.
716 Milligan G (2003) Constitutive Activity and Inverse Agonists of G Protein-Coupled Receptors: a Current
717 Perspective. Molecular Pharmacology 64:1271-1276.
718 Monyer H, Burnashev N, Laurie DJ, Sakmann B, Seeburg PH (1994) Developmental and regional
719 expression in the rat brain and functional properties of four NMDA receptors. Neuron 12:529-
720 540.
721 Moutin E, Raynaud F, Roger J, Pellegrino E, Homburger V, Bertaso F, Ollendorff V, Bockaert J, Fagni L,
722 Perroy J (2012) Dynamic remodeling of scaffold interactions in dendritic spines controls synaptic
723 excitability. The Journal of cell biology 198:251-263.
724 Müller A, Kukley M, Stausberg P, Beck H, Müller W, Dietrich D (2005) Endogenous Ca2+ buffer
725 concentration and Ca2+ microdomains in hippocampal neurons. The Journal of neuroscience : the
726 official journal of the Society for Neuroscience 25:558-565.
727 Naie K, Manahan-Vaughan D (2004) Regulation by metabotropic glutamate receptor 5 of LTP in the
728 dentate gyrus of freely moving rats: relevance for learning and memory formation. Cerebral
729 cortex (New York, NY : 1991) 14:189-198.
730 Nakazawa K, Jeevakumar V, Nakao K (2017) Spatial and temporal boundaries of NMDA receptor
731 hypofunction leading to schizophrenia. npj Schizophrenia 3:7.
732 O'Riordan KJ, Hu NW, Rowan MJ (2018) Physiological activation of mGlu5 receptors supports the ion
733 channel function of NMDA receptors in hippocampal LTD induction in vivo. Scientific reports
734 8:4391.
735 Paoletti P, Bellone C, Zhou Q (2013) NMDA receptor subunit diversity: impact on receptor properties,
736 synaptic plasticity and disease. Nature reviews Neuroscience 14:383-400.
737 Patrick B, Anne B, Amina R, Dimitri G, Michel K (1999) Differential interaction of the tSXV motifs of the
738 NR1 and NR2A NMDA receptor subunits with PSD-95 and SAP97. European Journal of
739 Neuroscience 11:2031-2043.
740 Pin JP, Acher F (2002) The metabotropic glutamate receptors: structure, activation mechanism and
741 pharmacology. Curr Drug Targets CNS Neurol Disord 1:297-317.
742 Polese D, de Serpis AA, Ambesi-Impiombato A, Muscettola G, de Bartolomeis A (2002) Homer 1a gene
743 expression modulation by antipsychotic drugs: involvement of the glutamate metabotropic
744 system and effects of D-cycloserine. Neuropsychopharmacology 27:906-913.
745 Rossi P, D'Angelo E, Taglietti V (1996) Differential long-lasting potentiation of the NMDA and non-NMDA
746 synaptic currents induced by metabotropic and NMDA receptor coactivation in cerebellar granule
747 cells. The European journal of neuroscience 8:1182-1189.
748 Shiraishi Y, Mizutani A, Mikoshiba K, Furuichi T (2003) Coincidence in dendritic clustering and synaptic
749 targeting of homer proteins and NMDA receptor complex proteins NR2B and PSD95 during
750 development of cultured hippocampal neurons. Molecular and Cellular Neuroscience 22:188-201.
751 Shiraishi Y, Mizutani A, Yuasa S, Mikoshiba K, Furuichi T (2004) Differential expression of Homer family
752 proteins in the developing mouse brain. The Journal of comparative neurology 473:582-599.

753 Skeberdis VA, Lan J, Opitz T, Zheng X, Bennett MV, Zukin RS (2001) mGluR1-mediated potentiation of
754 NMDA receptors involves a rise in intracellular calcium and activation of protein kinase C.
755 Neuropharmacology 40:856-865.
756 Spampanato J, Sullivan RK, Turpin FR, Bartlett PF, Sah P (2012) Properties of doublecortin expressing
757 neurons in the adult mouse dentate gyrus. PLoS One 7:e41029.
758 Steullet P, Cabungcal J, Monin A, Dwir D, O'Donnell P, Cuenod M, Do K (2016) Redox dysregulation,
759 neuroinflammation, and NMDA receptor hypofunction: A “central hub” in schizophrenia
760 pathophysiology? Schizophrenia research 176:41-51.
761 Sylantyev S, Rusakov DA (2013) Sub-millisecond ligand probing of cell receptors with multiple solution
762 exchange. Nature protocols 8:1299-1306.
763 Sylantyev S, Savtchenko LP, Ermolyuk Y, Michaluk P, Rusakov DA (2013) Spike-driven glutamate
764 electrodiffusion triggers synaptic potentiation via a homer-dependent mGluR-NMDAR link.
765 Neuron 77:528-541.
766 Szumlinski KK, Lominac KD, Kleschen MJ, Oleson EB, Dehoff MH, Schwartz MK, Seeberg PH, Worley PF,
767 Kalivas PW (2005) Behavioral and neurochemical phenotyping of Homer1 mutant mice: possible
768 relevance to schizophrenia. Genes, Brain and Behavior 4:273-288.
769 Toni N, Teng EM, Bushong EA, Aimone JB, Zhao C, Consiglio A, van Praag H, Martone ME, Ellisman MH,
770 Gage FH (2007) Synapse formation on neurons born in the adult hippocampus. Nat Neurosci
771 10:727-734.
772 Tu JC, Xiao B, Naisbitt S, Yuan JP, Petralia RS, Brakeman P, Doan A, Aakalu VK, Lanahan AA, Sheng M,
773 Worley PF (1999) Coupling of mGluR/Homer and PSD-95 complexes by the Shank family of
774 postsynaptic density proteins. Neuron 23:583-592.
775 Turrigiano G, Abbott LF, Marder E (1994) Activity-dependent changes in the intrinsic properties of
776 cultured neurons. Science (New York, NY) 264:974-977.
777 Williams NM, Preece A, Spurlock G, Norton N, Williams HJ, McCreadie RG, Buckland P, Sharkey V,
778 Chowdari KV, Zammit S (2004) Support for RGS4 as a susceptibility gene for schizophrenia.
779 Biological psychiatry 55:192-195.

780

781

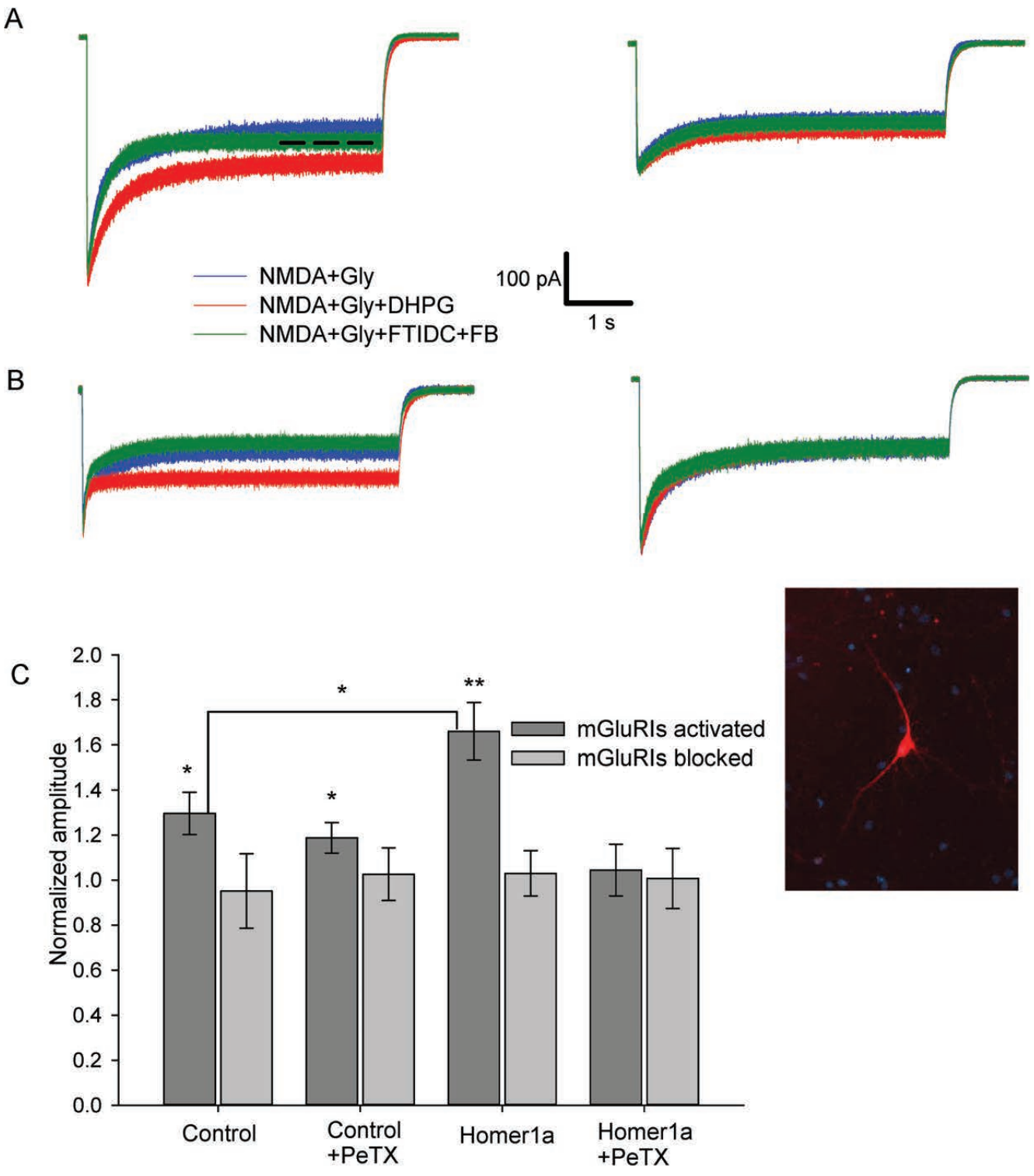

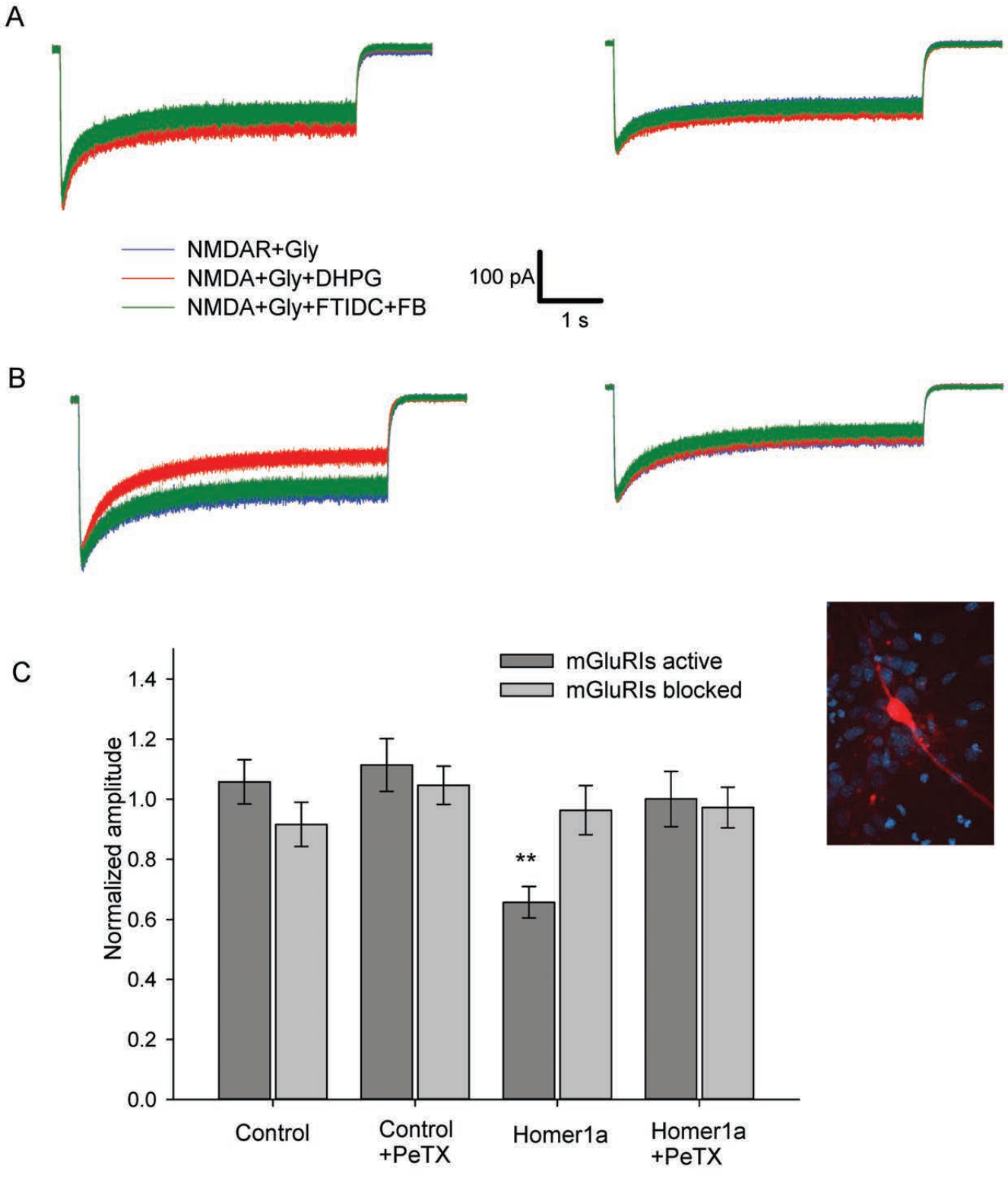

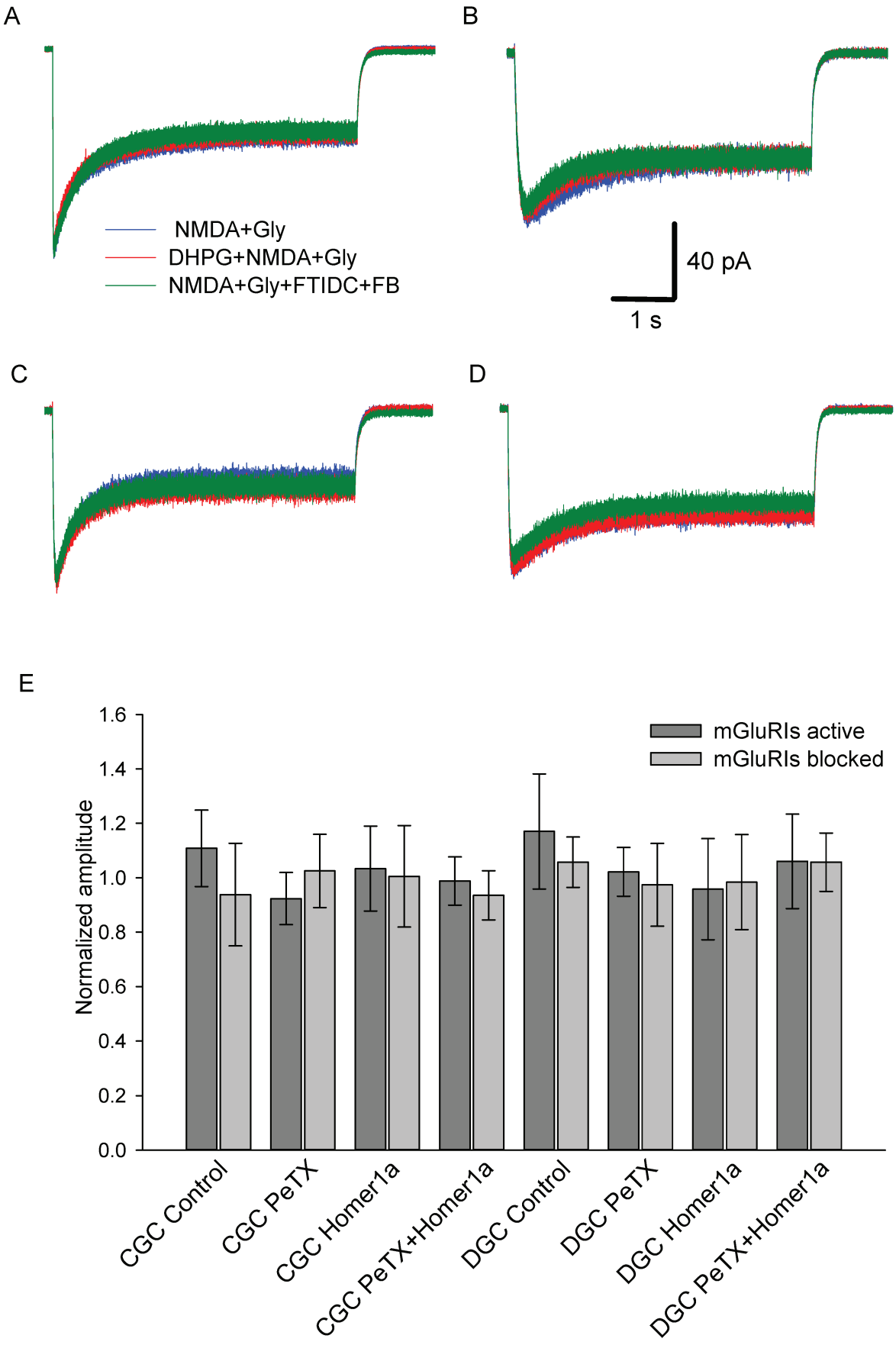

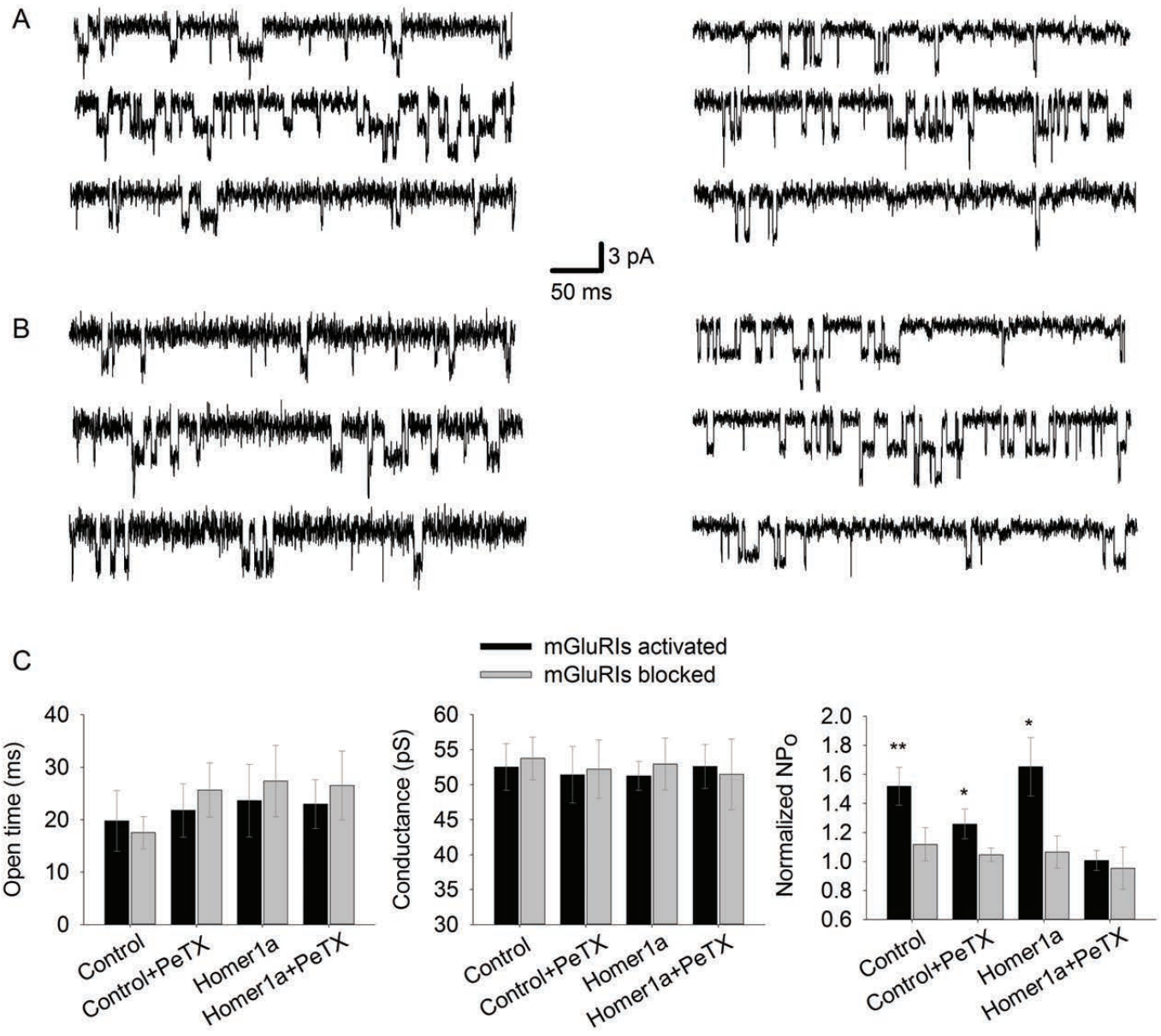

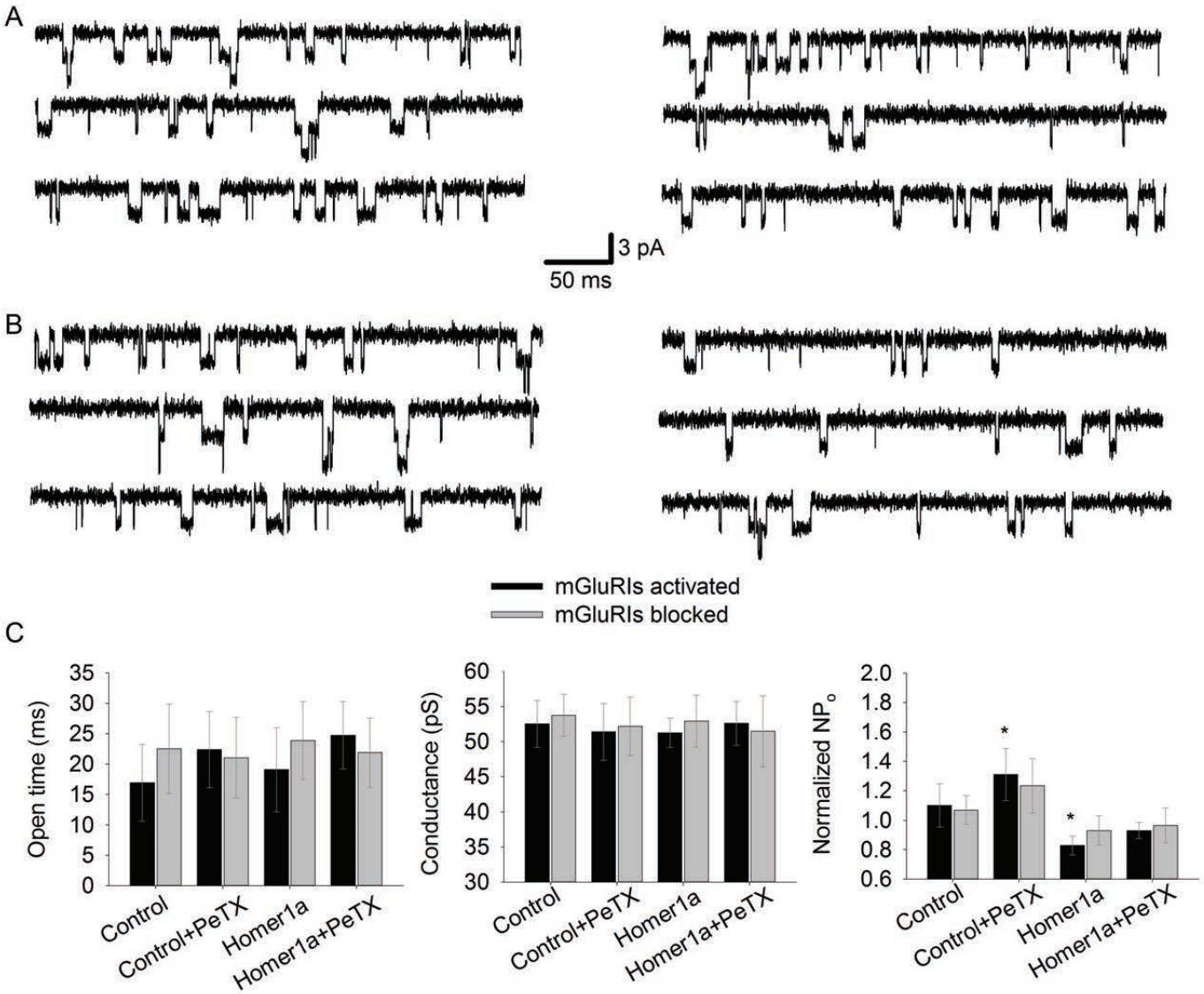

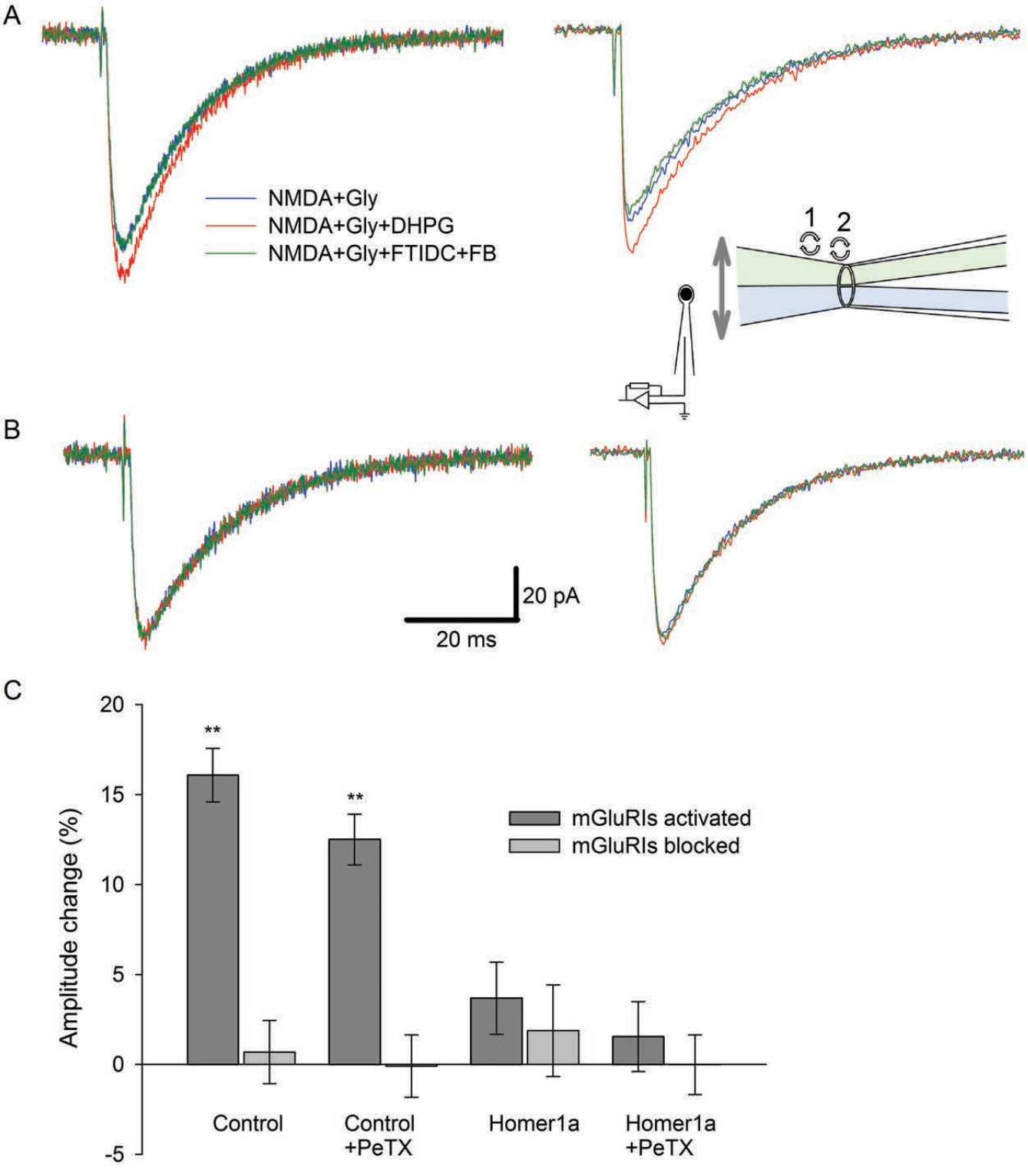

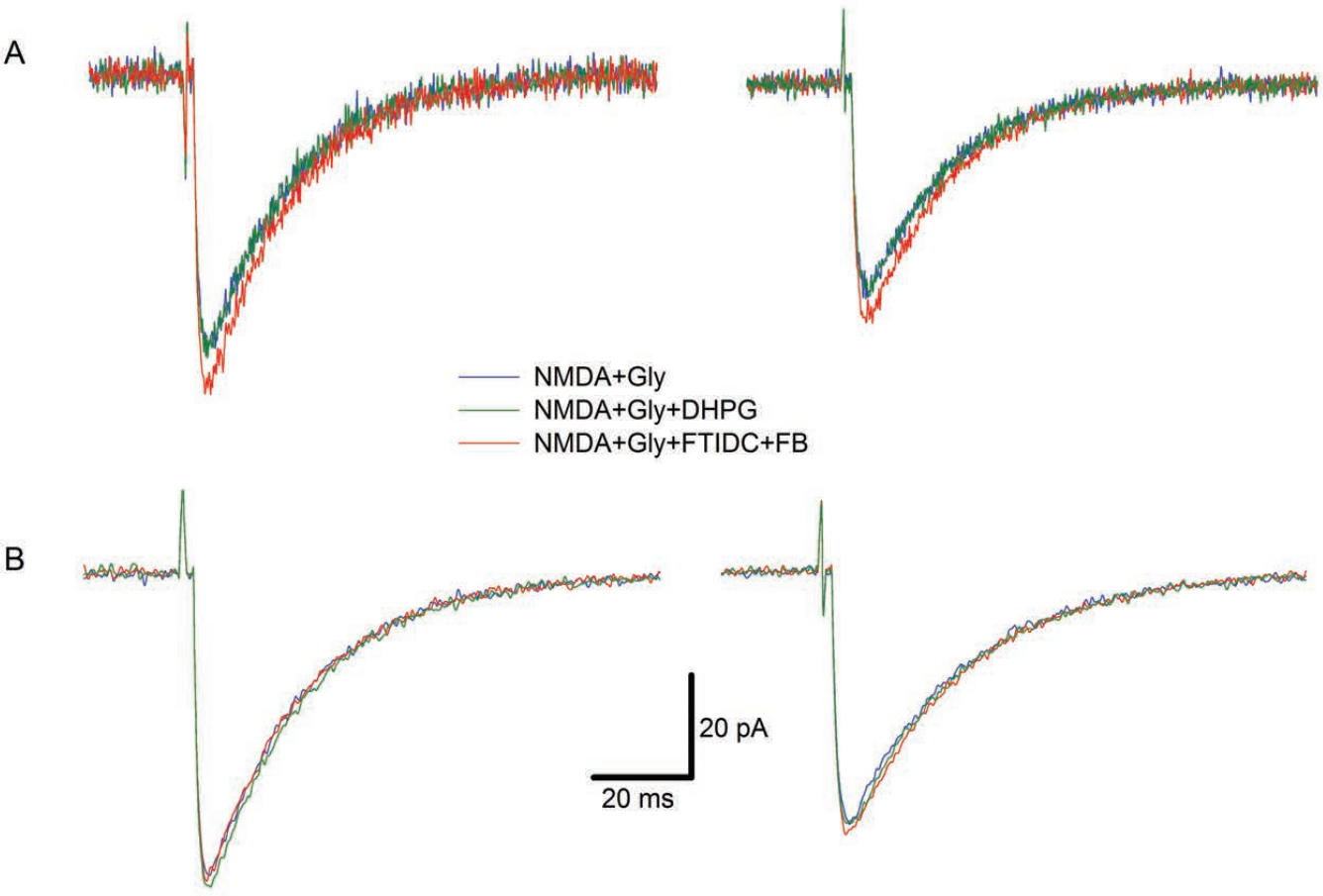

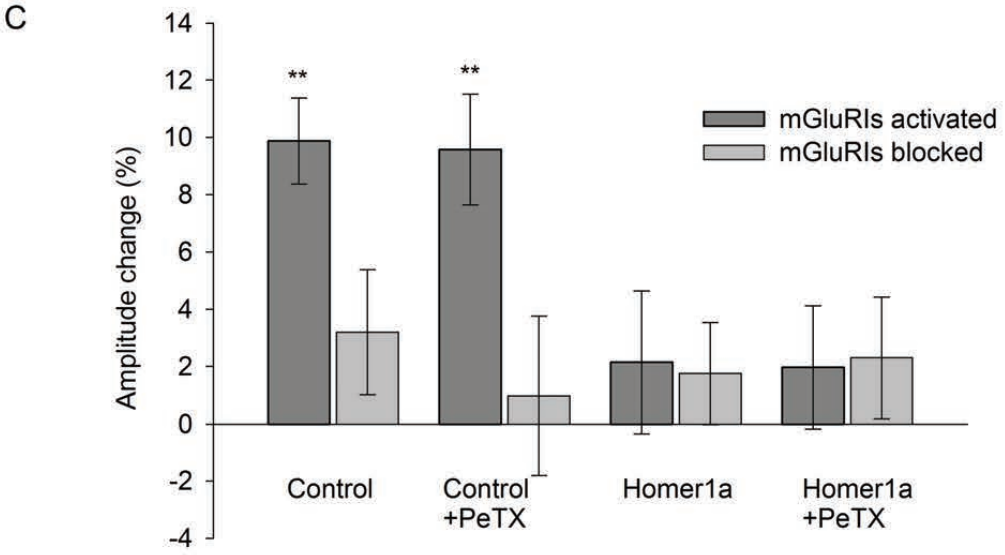

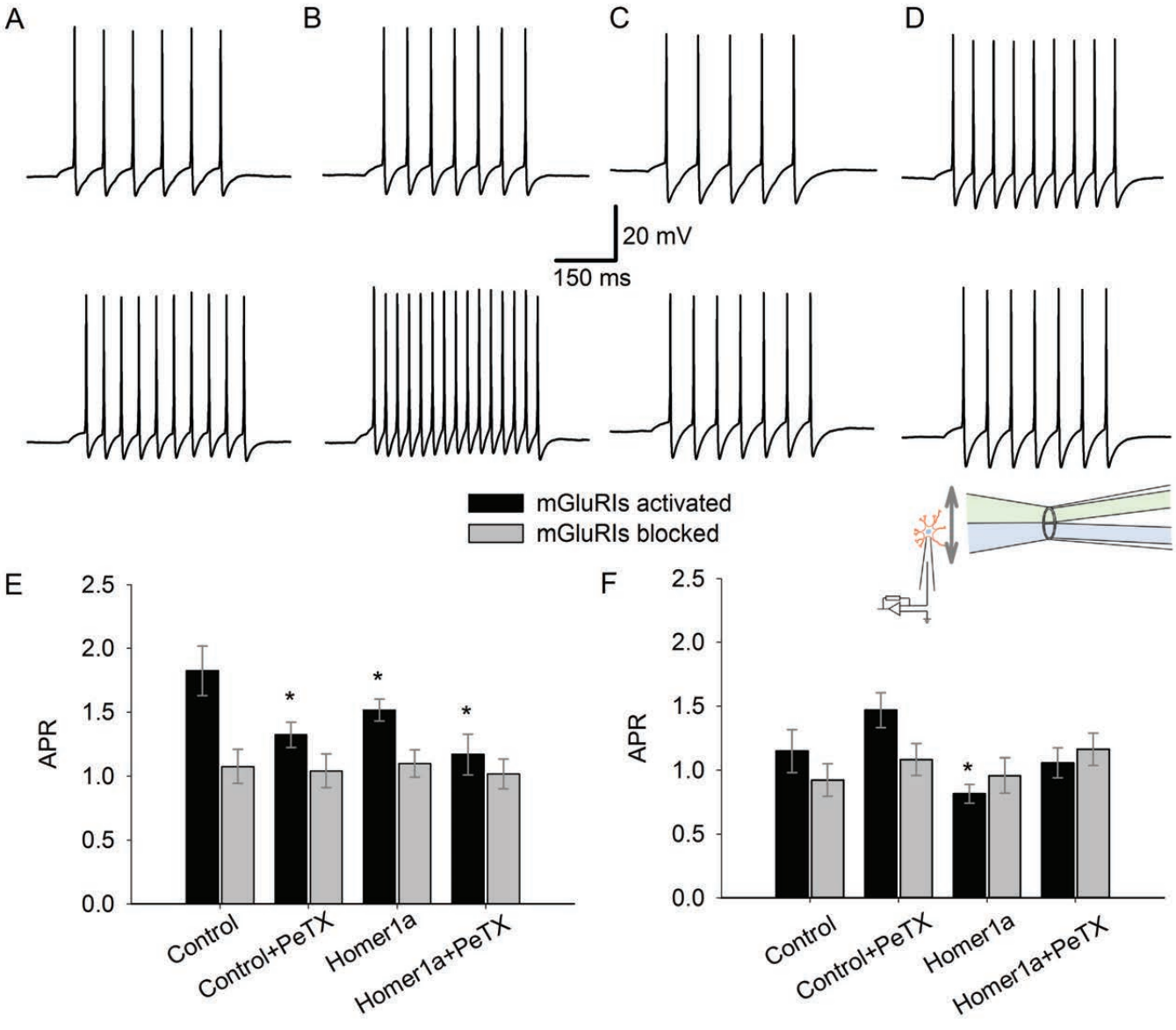

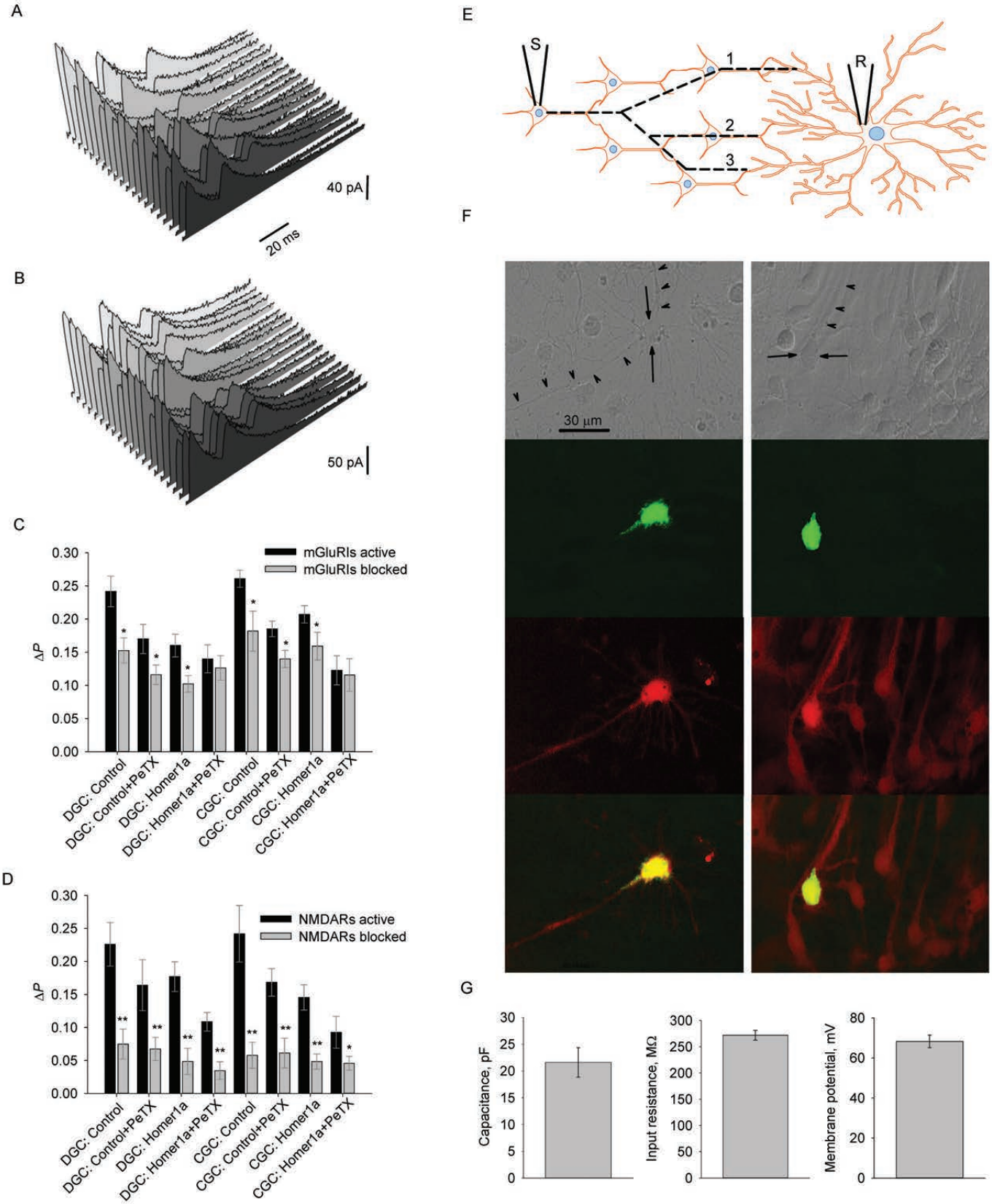

Figure 9